ChemComm

# Competition Between Side-Chain Interactions Dictates 2D Polymer Stacking Order



| | |
|---|---|
| Journal: | *ChemComm* |
| Manuscript ID | CC-COM-02-2023-001016.R1 |
| Article Type: | Communication |
| | |

COMMUNICATION

# Competition Between Side-Chain Interactions Dictates 2D Polymer Stacking Order

Alexander K. Oanta, Chloe E. Pelkowski, Michael J. Strauss, and William R. Dichtel*

Received 00th January 20xx,
Accepted 00th January 20xx

DOI: 10.1039/x0xx00000x

**Interrogating the stacking of two-dimensional polymers (2DPs) as a function of chemical composition is important to leverage their properties. We explore the dependence of 2DP crystallinity and porosity on variable amounts of zwitterions contained within the pores and find that high zwitterion loadings consistently diminish 2DP materials quality. A competition between disruptive zwitterion electrostatic forces and alkyl stabilization directs the stacking order of each 2DP and demonstrates the contrasting effects of side chain composition on COF crystallinity.**

Two-dimensional polymers are crystalline, porous network polymers with tunable topologies and functionalities stemming from careful monomer design.[1] 2DPs, especially the subclass known as 2D covalent organic frameworks (COFs), have been investigated for catalysis,[2, 3] gas storage,[4, 5] and molecular separations,[6, 7] and more. The appeal of 2DPs in these applications stems from the unique combination of structural features inherent to these materials, such as permanent porosity, the precise arrangement of functional groups, and readily-accessible 1D channels. However, fully leveraging 2DPs in these applications necessitates a fundamental understanding of how structural features impact stacking, as stacking order dictates pore accessibility and is necessary for high bulk crystallinity and porosity. Although 2DPs are often reported to have eclipsed stacking, offsets between layers can result in staggered stacking or slip-stacking wherein sheets can adapt unidirectional, alternating, or random offsets.[8]

Numerous methods involving installing motifs of varying sizes and/or charge states have been employed to understand how 2DP functionality directs the overall stacking order.[9-15] Installing zwitterionic moieties within the 2DP pores, which can yield a high ion density within these nanometer-scale channels, has yet to be thoroughly explored. There are a few examples of zwitterionic 2DPs that contain at least one charge located along the backbone,[16-18] as well as several charged 2DPs that have untethered counterions in the pores.[19, 20] Only one 2DP example has zwitterionic moieties contained entirely within dangling chains in the pores, but this system was not thoroughly investigated for structural changes arising from the installation of these groups.[21] Here we incorporate zwitterionic groups into 2DP pores with high yields and variable loadings and demonstrate that zwitterion loading has a destabilizing effect on the apparent crystallinity and porosity of the 2DP. The stacking order was found to diminish above certain zwitterion loading threshold values for the two different 2DP systems examined. These results demonstrate that alkyl chains stabilize the stacking interactions of layered 2DPs, and that interlayer interactions and resulting stacking order can be manipulated by including variable amounts of zwitterions.

Zwitterionic 2DPs were prepared by the post-polymerization reaction of dimethylamine-functionalized 2DPs with 1,3-propane sultone, as this ring-opening reaction[22, 23] introduced zwitterionic moieties into the 2DP pores. The acid-catalyzed condensation[24] of 2,5-bis(2-(dimethylamino)ethoxy)

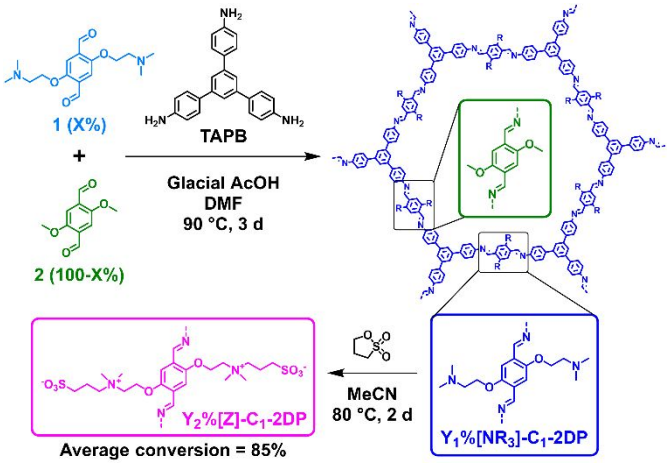


**Scheme 1** Synthesis of zwitterionic 2DPs.

*Department of Chemistry, Northwestern University, Evanston, Illinois 60208, United States. Email: wdichtel@northwestern.edu*
† Footnotes relating to the title and/or authors should appear here.
Electronic Supplementary Information (ESI) available: [details of any supplementary information available should be included here]. See DOI: 10.1039/x0xx00000x

terephthalaldehyde (**1**) with 1,3,5-tris(4-aminophenyl)benzene (TAPB) yielded dimethylamine-functionalized **100%[NR$_3$]-2DP** as a polycrystalline powder after activation (**Scheme 1**). Fourier-transform infrared spectroscopy (FT-IR) indicated that the product was imine-linked. This assignment was based on the appearance of a peak corresponding to the imine stretching frequency (1590 cm$^{-1}$) and concomitant loss of the features corresponding to the amine (3350 cm$^{-1}$) and the aldehyde (1680 cm$^{-1}$) monomers (**Figure S41**). These spectral features are consistent with conventional imine-linked 2DP syntheses.[25] Powder X-ray diffraction (PXRD) data corroborate predictions that describe hexagonal-pore **100%[NR$_3$]-2DP** forming with an average-eclipsed stacking geometry, with reflections at 2θ = 2.7° and 5.4° assigned to the (100) and (200) crystallographic planes, respectively (**Figure 1A**).[26] $N_2$ porosimetry experiments yield a type IV sorption isotherm, corresponding to a Brunauer-Emmett-Teller surface area ($S_{BET}$) of 870 m$^2$ g$^{-1}$ (**Figure 1B**). Taken together, these structural characterization data demonstrate that **100%[NR$_3$]-2DP** was synthesized as a high-quality microcrystalline powder.

Zwitterionic moieties were efficiently installed in the 2DP pores by functionalizing the pendant dimethylamine groups. **100%[NR$_3$]-2DP** was reacted with 1,3-propane sultone at 80 °C for 2 days in acetonitrile to install the zwitterions (**Scheme 1**).[23] To evaluate the efficiency of the ring-opening reaction, the insoluble 2DP product was hydrolyzed in DCl/$D_2O$ to return its

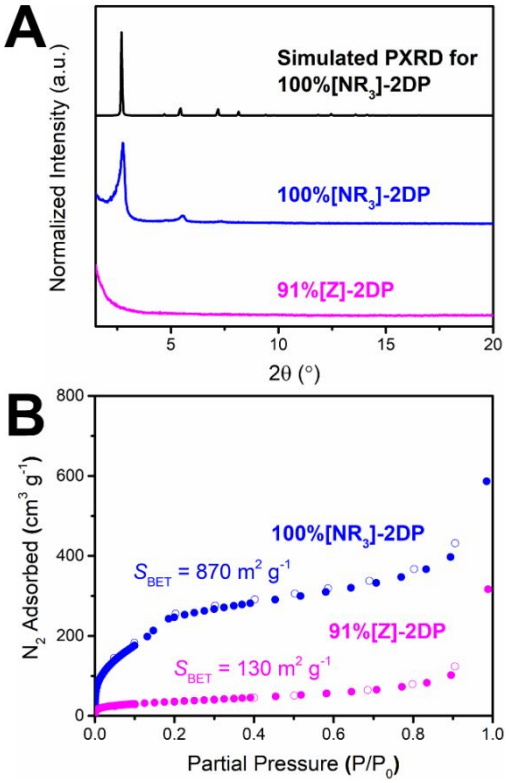


**Figure 1**. Synthesis and characterization of **100%[NR$_3$]-2DP** (blue) and the zwitterionic product of the subsequent reaction with 1,3-propane sultone, **91%[Z]-2DP** (pink). **(A)** Normalized PXRD patterns, and **(B)** $N_2$ sorption isotherms. In the PXRD patterns, the rise to the left of 2θ = 2.0° is due to instrument cutoff. 91% is the highest zwitterion loading achieved starting from **100%[NR$_3$]-2DP**, as quantified from $^1$H NMR digestion studies.

aldehyde-containing monomers as a mixture of **1** and its corresponding zwitterionic analogue. Comparing the integration values of the resonances from each dialdehyde using $^1$H Nuclear Magnetic Resonance (NMR) spectroscopy indicated that 91% of the original dimethylamine moieties reacted with the sultone (see **ESI** for a detailed discussion). The high efficiency of this post-polymerization transformation furnished a 2DP where 91% of the possible pore appendages were zwitterionic, and the remaining 9% were unreacted dimethylamine moieties, termed **91%[Z]-2DP**. This finding is consistent with reports of tertiary amines reacting with 1,3-propane sultone to high conversion.[22, 23] **91%[Z]-2DP** also exhibited changes in its solid-state $^{13}$C cross-polarization magic angle spinning (CP-MAS) NMR spectrum relative to its precursor **100%[NR$_3$]-2DP** that were similar to the spectrum of a zwitterionic model compound (**Figure S46**). The efficiency of the post-polymerization functionalization of **100%[NR$_3$]-2DP** enabled subsequent systematic investigations into how zwitterionic pore functionality can impact 2DP stacking.

The installation of zwitterionic moieties within the 2DP pores was accompanied by a notable reduction in the crystallinity and porosity of the material. The PXRD pattern of the **91%[Z]-2DP** product displays a loss of crystallinity, with no defined Bragg features present (**Figure 1A**). Additionally, the $N_2$ sorption isotherm of the material revealed a marked decrease of the surface area to 130 m$^2$ g$^{-1}$ (**Figure 1B**). A high mass yield (94%) of the transformation was observed, ruling out the possibility of partial exfoliation, and FT-IR and $^{13}$C CP-MAS NMR spectroscopies demonstrated that the imine linkages within the 2DP sheets are retained (**Figures S42, S46**). Scanning electron microscopy (SEM) images show that there are no significant morphological changes between **100%[NR$_3$]-2DP** and **91%[Z]-2DP** (**Figures S47, S48**). Taken together, these results suggest that the 2DP sheets with high zwitterion loading are still chemically intact but have lost their ability to stack in a periodic fashion. Ultimately, this loss of ordered stacking results in reduced crystalline signal and surface area.

2DPs with variable zwitterion loadings were synthesized to investigate the role of zwitterion loading on 2DP crystallinity and porosity. Dimethylamine linker **1** and 2,5-dimethoxyterephthalaldehyde **2** were reacted with TAPB using varying aldehyde feed ratios (X = 0–100%) to yield crystalline dimethylamine-functionalized **Y$_1$%[NR$_3$]-C$_1$-2DP** products. In this notation, $Y_1$ corresponds to dimethylamine linker loading as determined by $^1$H NMR digestion of 2DP products (**Scheme 1**; see **ESI**). These 2DPs were reacted with 1,3-propane sultone to yield **Y$_2$%[Z]-C$_1$-2DP** products, and the final $Y_2$ zwitterion loadings were again quantified by acid digestion $^1$H NMR analyses and indicate an average dimethylamine-to-zwitterion conversion rate of 82%, with final nonzero zwitterion loadings ranging from 5-91%. For example, a **13%[Z]-C$_1$-2DP** product denotes that 13% of possible pore appendages are zwitterion moieties, while the remaining 87% of possible pore appendages are a combination of methoxy groups and a small amount of unreacted dimethylamine groups. These data indicate that a range of 2DP dimethylamine loadings, and subsequent zwitterion loadings, are accessible by this approach.

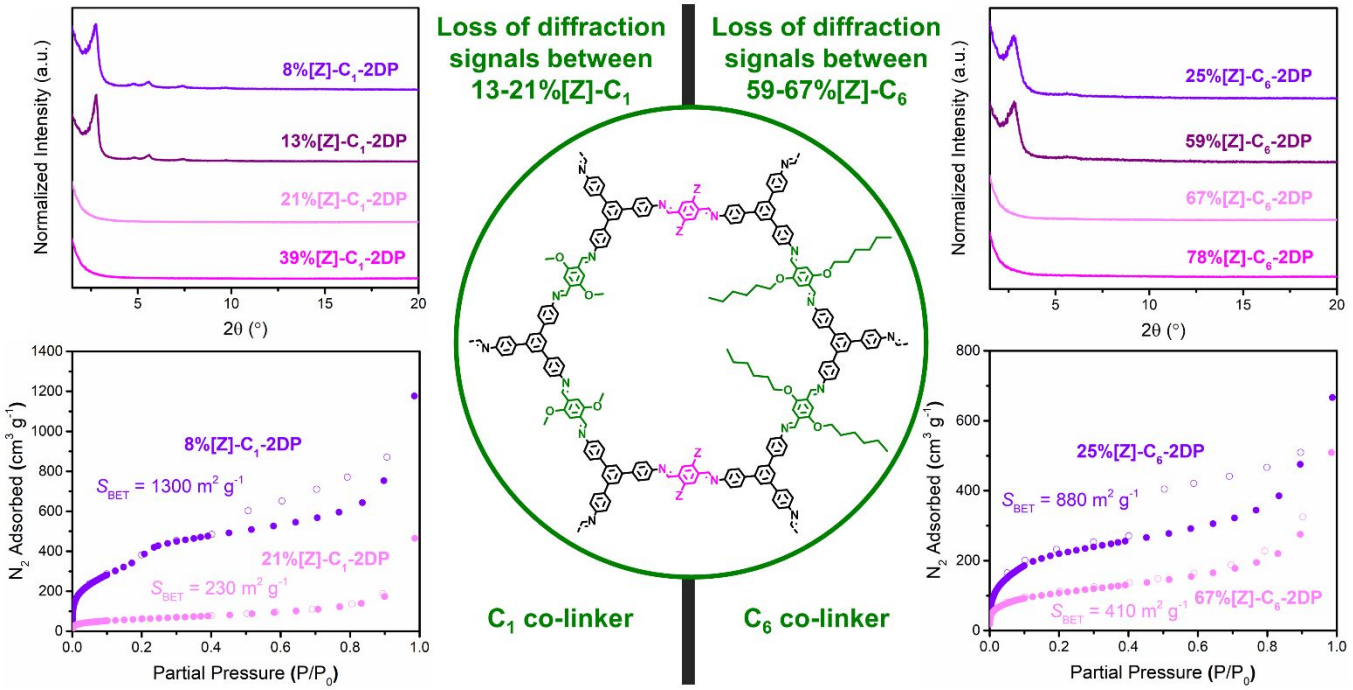


**Figure 2.** Structural characterization of variably-loaded **[Z]-$C_1$** (left) and **[Z]-$C_6$** (right) **2DP**s, where "Z" = zwitterionic chain in the chemical structure. Normalized PXRD patterns (top) and nitrogen sorption isotherms (bottom) of zwitterionic 2DPs, with final zwitterion loadings and $S_{BET}$ values indicated. In both systems, there is a zwitterion loading threshold above which the 2DP products lose structural order. 2DPs with zwitterion loadings below these thresholds all display crystalline features and possess high surface areas, while 2DPs with zwitterion loadings above these thresholds all display reduced crystallinity and surface areas, with nearly identical PXRD patterns and nitrogen isotherms. In the PXRD patterns, the rise to the left of 2θ = 2.0° is due to instrument cutoff. The 2DP loadings are all quantified through $^1$H NMR digestion studies.

Higher zwitterion loadings directly impact 2DP crystallinity and porosity, sharply reducing materials quality above a threshold level. At low zwitterion loadings (≤13%) the **$C_1$-2DP**s display crystalline signals *via* PXRD. However, at higher zwitterion loadings (≥21%) no 2DP exhibited features in its PXRD pattern, indicating that there is a zwitterion loading threshold value within 13-21%, below which apparent crystallinity is maintained, and above which crystallinity is diminished (**Figure 2**). $N_2$ porosimetry data is consistent with this finding: **8%[Z]-$C_1$-2DP** exhibits an $S_{BET}$ of 1300 $m^2$ $g^{-1}$, while that of the **21%[Z]-$C_1$-2DP** decreases to 230 $m^2$ $g^{-1}$ (**Figure 2**). This trend in surface area reduction is highlighted in a plot of surface area vs. zwitterion loading, reinforcing the observation of a zwitterion loading threshold impacting materials quality (**Figure 3**). The mass yields of all zwitterion-forming reactions are still high (>91%). This observation, along with crystallographic and porosimetry data, again suggests that high zwitterion loading leads to disordered sheet stacking as opposed to exfoliation.

Zwitterionic 2DPs made with a co-linker bearing a larger alkoxy group maintain high materials quality up to higher zwitterion loadings and still display an analogous zwitterion loading threshold effect. We prepared another series of dimethylamine-based 2DPs with 2,5-bis(hexyloxy) terephthalaldehyde as a co-linker. We hypothesized that the van der Waals interactions between stacked hexyloxy side chains would help favor interlayer sheet stacking despite high neighboring zwitterion content. Combining **1** and 2,5-bis(hexyloxy)terephthalaldehyde with TAPB furnished **$Y_1$%[$NR_3$]-$C_6$-2DP** products that served as high quality precursors (**Scheme 1**; see **ESI**) to form $C_6$-based zwitterionic 2DPs using our ring-opening method. These precursor 2DPs were accordingly reacted with 1,3-propane sultone to yield zwitterionic **$Y_2$%[Z]-$C_6$-2DP** products, with an average dimethylamine-to-zwitterion conversion rate of 91% and final nonzero zwitterion loadings ranging from 25-78%. In a manner analogous to that of the $C_1$ 2DP series, here the $C_6$ 2DPs display crystalline signals via PXRD at zwitterion loadings ≤59%, but not at higher loadings (≥67%), indicating a zwitterion loading threshold value within 59-67% below which crystallinity is retained, and above which crystallinity is lost (**Figure 2**). Nitrogen porosimetry experiments corroborate this threshold finding, as **25%[Z]-$C_6$-2DP** possesses a $S_{BET}$ of 880 $m^2$ $g^{-1}$, while **67%[Z]-$C_1$-2DP** decreases to 410 $m^2$ $g^{-1}$ (**Figure 2**).

The maximum zwitterion loading in the **$C_6$-2DP** series (59–67%) while maintaining crystallinity is higher than that of the **$C_1$-2DP** series (13–21%), suggesting that the hexyloxy chains play a vital role in facilitating ordered interlayer sheet stacking. The observed drop in surface area is more drastic in the zwitterionic **$C_1$-2DP** series relative to the zwitterionic **$C_6$-2DP** series. This observation has two potential rationales. First, the precursor dimethylamine-functionalized **$C_1$-2DP**s have higher surface areas than the parallel precursor **$C_6$-2DP**s, whereas their respective zwitterionic product 2DPs for both co-linkers have similar surface area values, making the $S_{BET}$ drop in **$C_1$-2DP**s more pronounced. Second, the methoxy chains proved far less effective than the hexyloxy chains in promoting an ordered assembly of zwitterion-functionalized 2DP sheets – even at very low loadings – so the **$C_1$-2DP**s lose interlayer stacking order at a

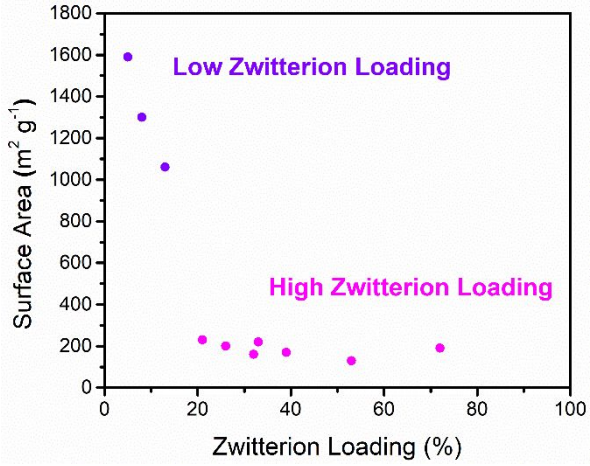


**Figure 3.** Surface areas as a function of zwitterion loading for the **$Y_2$%[Z]-$C_1$-2DP**s. A dramatic drop of $S_{BET}$ values is seen around the zwitterionic loading threshold (13-21%), and the $S_{BET}$ values remain relatively constant above the threshold.

much lower zwitterion loading. Overall, we find a competition between disruptive zwitterion electrostatic forces and alkyl stabilization that dictates the stacking order of each 2DP.

In conclusion, we have found that zwitterions loaded into the pores of 2DPs disrupt the sheet stacking order. Dimethylamine-functionalized 2DPs are converted to zwitterionic 2DPs in high yields and at variable loadings. Zwitterionic 2DPs made with either methoxy or hexyloxy co-linkers demonstrate a similar trend: below a certain threshold of zwitterion loading, the 2DP maintains stacking order and exhibits high crystallinity and porosity, whereas above that loading threshold these properties diminish. The hexyloxy 2DPs can maintain stacking order at higher zwitterion loadings than can the methoxy 2DPs, highlighting that there is a competition between deleterious zwitterion electrostatic interactions and alkyl stabilization forces that directs the stacking order of each 2DP. This study furthers our understanding of 2DP stacking parameters and provides another avenue to direct 2DP interlayer interactions.

This study was supported by the Strategic Environmental Research and Development Program (ER18-1026). M. J. S. was supported by the NSF GRFP (DGE-11842165). This work made use of the IMSERC at Northwestern University, which has received support from the Soft and Hybrid Nanotechnology Experimental (SHyNE) Resource (NSF ECCS-1542205 and NSF ECCS-2025633), the State of Illinois, and the International Institute for Nanotechnology (IIN). The authors warmly thank Leslie S. Hamachi, Benjamin R. Elling, and Omar K. Farha for insightful discussions and helpful feedback.

## Conflicts of interest

There are no conflicts to declare.

## Notes and references

1. K. Geng, T. He, R. Liu, S. Dalapati, K. T. Tan, Z. Li, S. Tao, Y. Gong, Q. Jiang and D. Jiang, *Chem. Rev.*, 2020, **120**, 8814-8933.
2. S.-Y. Ding, J. Gao, Q. Wang, Y. Zhang, W.-G. Song, C.-Y. Su and W. Wang, *J. Am. Chem. Soc.*, 2011, **133**, 19816-19822.
3. H. Xu, J. Gao and D. Jiang, *Nat. Chem.*, 2015, **7**, 905-912.
4. H. Furukawa and O. M. Yaghi, *J. Am. Chem. Soc.*, 2009, **131**, 8875-8883.
5. Y. Yang, M. Faheem, L. Wang, Q. Meng, H. Sha, N. Yang, Y. Yuan and G. Zhu, *ACS Cent. Sci.*, 2018, **4**, 748-754.
6. H. Wang, Y. Zhai, Y. Li, Y. Cao, B. Shi, R. Li, Z. Zhu, H. Jiang, Z. Guo, M. Wang, L. Chen, Y. Liu, K.-G. Zhou, F. Pan and Z. Jiang, *Nat. Commun.*, 2022, **13**, 7123.
7. S. Yuan, X. Li, J. Zhu, G. Zhang, P. Van Puyvelde and B. Van der Bruggen, *Chem. Soc. Rev.*, 2019, **48**, 2665-2681.
8. A. M. Pütz, M. W. Terban, S. Bette, F. Haase, R. E. Dinnebier and B. V. Lotsch, *Chem. Sci.*, 2020, **11**, 12647-12654.
9. X. Wu, X. Han, Y. Liu, Y. Liu and Y. Cui, *J. Am. Chem. Soc.*, 2018, **140**, 16124-16133.
10. X. Chen, M. Addicoat, S. Irle, A. Nagai and D. Jiang, *J. Am. Chem. Soc.*, 2013, **135**, 546-549.
11. S. B. Alahakoon, S. D. Diwakara, C. M. Thompson and R. A. Smaldone, *Chem. Soc. Rev.*, 2020, **49**, 1344-1356.
12. T. Sick, J. M. Rotter, S. Reuter, S. Kandambeth, N. N. Bach, M. Döblinger, J. Merz, T. Clark, T. B. Marder, T. Bein and D. D. Medina, *J. Am. Chem. Soc.*, 2019, **141**, 12570-12581.
13. M. Martínez-Abadía and A. Mateo-Alonso, *Adv. Mater.*, 2020, **32**, 2002366.
14. F. Haase, K. Gottschling, L. Stegbauer, L. S. Germann, R. Gutzler, V. Duppel, V. S. Vyas, K. Kern, R. E. Dinnebier and B. V. Lotsch, *Mater. Chem. Front.*, 2017, **1**, 1354-1361.
15. S. B. Alahakoon, K. Tan, H. Pandey, S. D. Diwakara, G. T. McCandless, D. I. Grinffiel, A. Durand-Silva, T. Thonhauser and R. A. Smaldone, *J. Am. Chem. Soc.*, 2020, **142**, 12987-12994.
16. Y. Li, H. Wu, Y. Yin, L. Cao, X. He, B. Shi, J. Li, M. Xu and Z. Jiang, *J. Membr. Sci.*, 2018, **568**, 1-9.
17. Y. Fu, Y. Wu, S. Chen, W. Zhang, Y. Zhang, T. Yan, B. Yang and H. Ma, *ACS Nano*, 2021, **15**, 19743-19755.
18. Y. Wang, S. Geng, G. Yan, X. Liu, X. Zhang, Y. Feng, J. Shi and X. Qu, *ACS Appl. Energy Mater.*, 2022, **5**, 2495-2504.
19. R. Z. Lange, G. Hofer, T. Weber and A. D. Schlüter, *J. Am. Chem. Soc.*, 2017, **139**, 2053-2059.
20. B. Dong, L. Wang, S. Zhao, R. Ge, X. Song, Y. Wang and Y. Gao, *Chem. Commun.*, 2016, **52**, 7082-7085.
21. Z.-J. Mu, X. Ding, Z.-Y. Chen and B.-H. Han, *ACS Appl. Mater. Interfaces*, 2018, **10**, 41350-41358.
22. M. K. Vasudevamurthy, M. Lever, P. M. George and K. R. Morison, *Biopolymers*, 2009, **91**, 85-94.
23. Z. A. Page, Y. Liu, E. Puodziukynaite, T. P. Russell and T. Emrick, *Macromolecules*, 2016, **49**, 2526-2532.
24. J. I. Feldblyum, C. H. McCreery, S. C. Andrews, T. Kurosawa, E. J. Santos, V. Duong, L. Fang, A. L. Ayzner and Z. Bao, *Chem. Commun.*, 2015, **51**, 13894-13897.
25. B. J. Smith, A. C. Overholts, N. Hwang and W. R. Dichtel, *Chem. Commun.*, 2016, **52**, 3690-3693.
26. W. Ji, L. Xiao, Y. Ling, C. Ching, M. Matsumoto, R. P. Bisbey, D. E. Helbling and W. R. Dichtel, *J. Am. Chem. Soc.*, 2018, **140**, 12677-12681.